hydrology

MDPI

Article

Quantifying Baseflow with Radon, H and O Isotopes and Field Parameters in the Urbanized Catchment of the Little Jukskei River, Johannesburg

Khutjo Diphofe [1,†], Roger Diamond [2,*] and Francois Kotze [1,‡]

[1] Department of Geology, University of Pretoria, Hatfield, Pretoria 0028, South Africa; khutjo.d@umvoto.com (K.D.); francois@geostratum.co.za (F.K.)
[2] BIOGRIP (Biogeochemistry Research Infrastructure Platform), Department of Geological Sciences, University of Cape Town, Rondebosch, Cape Town 7700, South Africa
* Correspondence: roger.diamond@uct.ac.za
† Current address: Umvoto, 8 Beach Road, Muizenberg, Cape Town 7945, South Africa.
‡ Current address: Geostratum, Bethlehem 9700, South Africa.

Abstract

Understanding groundwater and surface water interaction is critical for managing water resources, particularly in water-stressed and rapidly urbanizing areas, such as many parts of Africa. A survey was conducted of borehole, spring, seep and river water radon, δ^2H, $\delta^{18}O$ and field parameters in the Jukskei River catchment, Johannesburg. Average values of electrical conductivity (EC) were 274 and 411 $\mu S \cdot cm^{-1}$ for groundwater and surface water, and similarly for radon, 37,000 and 1100 $Bq \cdot m^{-3}$, with a groundwater high of 196,000 $Bq \cdot m^{-3}$ associated with a structural lineament. High radon was a good indicator of baseflow, highest at the end of the rainy season (March) and lowest at the end of the dry season (September), with the FINIFLUX model computing groundwater inflow as 2.5–4.7 $L \cdot m^{-1} s^{-1}$. High EC was a poorer indicator of baseflow, also considering the possibility of wastewater with high EC, typical in urban areas. Groundwater δ^2H and $\delta^{18}O$ values are spread widely, suggesting recharge from both normal and unusual rainfall periods. A slight shift from the local meteoric water line indicates light evaporation during recharge. Surface water δ^2H and $\delta^{18}O$ is clustered, pointing to regular groundwater input along the stream, supporting the findings from radon. Given the importance of groundwater, further study using the same parameters or additional analytes is advisable in the urban area of Johannesburg or other cities.

Keywords: urban hydrology; baseflow; stable isotopes; radon; Johannesburg

Academic Editor: Yong Xiao

Received: 18 June 2025
Revised: 17 July 2025
Accepted: 19 July 2025
Published: 2 August 2025

Citation: Diphofe, K.; Diamond, R.; Kotze, F. Quantifying Baseflow with Radon, H and O Isotopes and Field Parameters in the Urbanized Catchment of the Little Jukskei River, Johannesburg. *Hydrology* **2025**, *12*, 203. https://doi.org/10.3390/hydrology12080203

1. Introduction

Understanding and quantifying groundwater contributions (baseflow) to urban rivers is crucial for sustainable water management, especially in rapidly urbanizing and water-stressed regions such as Johannesburg, South Africa [1–3]. In these environments, baseflow from groundwater plays a vital role in sustaining river systems during dry seasons, supporting both ecological health and urban water [4–6]. The temporal physiochemical variations in streams are primarily influenced by dominant seasonal sources. In urban catchments, natural sources such as tributaries, lakes and groundwater exert more influence during wetter seasons, whereas wastewater effluent and baseflow tend to be more prominent during dry seasons [7–9].

Research on baseflow contributions has increasingly leveraged natural tracers such as stable isotopes of hydrogen and oxygen, as well as radon (^{222}Rn), to delineate groundwater inputs into surface water systems. Radon, historically employed in oceanographic contexts, has proven effective for identifying and quantifying groundwater discharge in various hydrogeological settings [10–13]. While radon has been increasingly used to trace groundwater–surface water interactions globally, its application in fractured aquifers in South Africa remains limited and largely qualitative [14].

Stable isotopes, on the other hand, have been widely used to distinguish water sources, identify recharge mechanisms, and trace evaporation processes in both rural and urban catchments [15,16]. Urban hydrology adds further complexity due to impervious surfaces, leakage from infrastructure and high runoff rates that obscure natural hydrological signals [4,9,17]. The resulting challenge is a lack of quantitative data on baseflow dynamics within urban streams.

According to the statistical analyses by Le Maitre and Colvin [18], the correlations between river flow indices and rainfall patterns across South Africa are intricate. This intricacy is observable even within individual principal aquifer types, and it is connected to climate and the dispersion of less prevalent lithologies throughout a catchment.

This study applies a combined approach using radon-222, stable isotopes (δ^2H and δ^{18}O) and field parameters (EC, temperature, pH) to assess seasonal groundwater contributions to baseflow in the Little Jukskei River, an urban stream within Johannesburg. The study further applies the FINIFLUX model to estimate groundwater discharge into the river. This represents a novel application in the context of fractured crystalline aquifers in urban Africa and provides insights critical for sustainable urban water management.

Radon is a noble gas commonly found in rock, sediment and water, with a half-life of 3.82 days [19,20]. It is derived from the decay of ^{238}U, as shown in Figure 1, engrained in rock and sediment. Radon accumulates in groundwater due to cooler temperatures, reduced degassing and greater emanation. In surface water, its concentration is influenced by tributary inflow, groundwater connection, sediment radon content, degassing and decay [21,22].

Groundwater discharge into surface water bodies can be traced by monitoring the radon concentration. The conventional method of utilizing radon to estimate groundwater flux involves directly solving the ordinary differential equation for radon mass balance (1) across small discretized stream reaches [11,23]. The mass balance parameters are expanded in Table 1. Discrete point concentrations serve as input for inverted forward modelling, aiming to estimate various unknown parameters such as groundwater inflow (I) and hyporheic exchange.

$$Q_s \frac{\delta c}{\delta x} = I\left(c_{gw} - c\right) - kwdc - dwc\lambda_{Rn} + \alpha_1 - \alpha_2 c \quad (1)$$

Table 1. Description and units for the parameters of the radon surface water–groundwater mass balance in Equation (1).

Parameter	Description	Units	Comments
Q_s	streamflow rate	$m^3 \cdot d^{-1}$	measured
I	groundwater inflow	$m^3 \cdot d^{-1}$	calculated
x	stream length	m	measured
w	stream width	m	measured
d	stream depth	m	measured
c	stream radon concentration	$Bq \cdot m^{-3}$	measured
c_{gw}	groundwater radon concentration	$Bq \cdot m^{-3}$	measured

Table 1. *Cont.*

Parameter	Description	Units	Comments
k	gas exchange coefficient	$m^2 \cdot d^{-1}$	known constant
λ_{Rn}	first-order decay constant	d^{-1}	known constant
α_1	hyporheic kinetic production	$Bq \cdot m^{-3} \cdot d^{-1}$	calculated
α_2	hyporheic kinetic decay	$Bq \cdot m^{-3} \cdot d^{-1}$	calculated

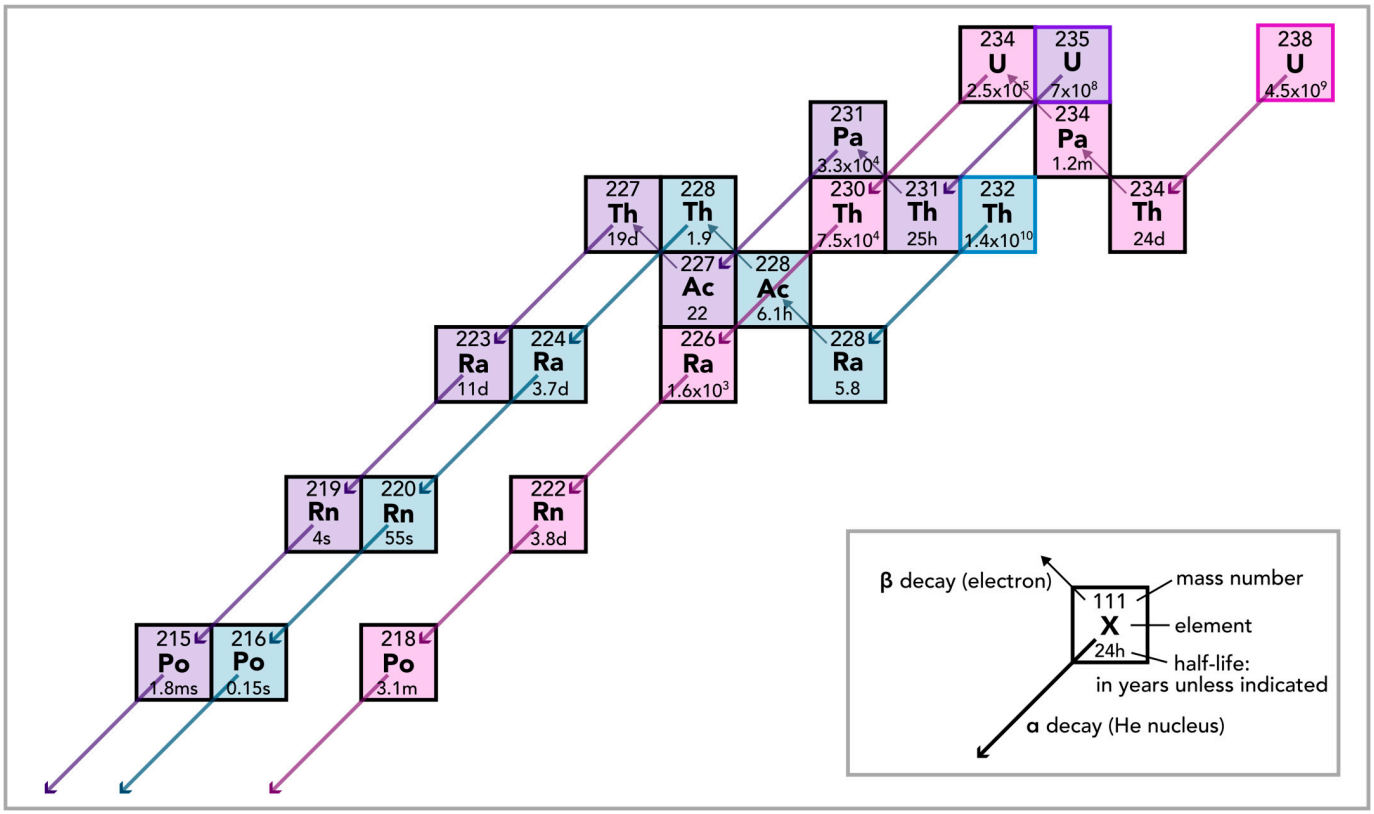

Figure 1. Radioactive decay chains for the three naturally occuring isotopes of radon. Due to short half-lives and lower abundance of the original parents, ^{219}Rn barely occurs and ^{220}Rn is rare, leaving ^{222}Rn as the main isotope. The long half-life primordial isotopes are outlined in colour. Being a noble gas, radon is ejected from the aquifer matrix and dissolves into the groundwater, but upon exposure to air, the radon is soon lost, so it acts as a useful tracer of recent groundwater discharge into surface waters.

While radon has been increasingly used to trace groundwater–surface water interactions globally, its application in fractured aquifers in South Africa remains limited and largely qualitative. For example, Strydom et al. (2021) [14] detected groundwater discharge zones in the fractured Table Mountain Group aquifers using radon, but the study did not attempt to estimate discharge magnitudes. This study applies radon measurements within the saturated zone and employs the FINIFLUX model to quantify groundwater fluxes directly. This approach represents a novel contribution by transitioning from qualitative detection to quantitative estimation of groundwater inputs in a highly urbanized catchment underlain by fractured crystalline aquifers in South Africa.

Perhaps the most commonly used natural tracers in environmental studies are the stable isotopes of water, namely hydrogen and oxygen. Among the many applications of these are groundwater–surface water interaction studies [15]. Stable isotopes have been utilized in urban catchments to distinguish various water sources, including groundwa-

ter, stormwater runoff, wastewater effluent and dams [9,17]. Additionally, they aid in determining the distribution patterns of water transit times [16].

The ratio of the heavy to light isotopes in a body of water, for example ^{18}O to ^{16}O in an aquifer, varies due to slightly different reaction rates of these isotopes during diffusion, phase transitions and chemical reactions. These processes are called fractionation and are affected by temperature and reaction conditions, such as humidity, wind speed and others [24]. In addition, obvious variations due to location, season and other spatial and temporal changes create a distribution of the stable isotope values across the landscape and in different water bodies. These differences can be used to track water flows [25]. In many cases, especially where surface water and groundwater have not travelled far since their origin as precipitation, the main source of isotope variations is inherited from precipitation factors, such as latitude, altitude, temperature, cloud height and evaporation during rainfall.

2. Study Area

2.1. Location

The study site is located in the Jukskei River catchment (JRC), within the area of greater Johannesburg in the centre of Gauteng Province (see Figure 2). The JRC belongs to the A21C quaternary catchment of the Crocodile West and Marico Water Management Area. Johannesburg occupies a watershed, with the JRC flowing into the Limpopo River in the north, while the Klip River catchment drains into the Vaal River in the south. Additionally, the JRC marks the southernmost point of the Upper Crocodile River Basin. Covering an area of roughly 750 km^2, the catchment comprises seven sub-catchments. The focus of this study is the Little Jukskei River catchment, which lies in the northwest of the JRC. Work was also done in the headwaters of the Braamfonteinspruit, which includes the tributary known as the Montgomeryspruit. The Braamfonteinspruit flows directly into the Jukskei River.

2.2. Geology

The geology features ~3.34 Ga greenstones [26], intruded by the ~3120 Ma Johannesburg Dome granitoids, comprising tonalite, granodiorite, gneiss and migmatite [27] (see Figure 3). A period of mafic intrusion followed the granite emplacement [28], and these dykes are visible in the northern half of the dome. The southern boundary of the Upper Crocodile River Basin is defined by the Witwatersrand Supergroup. The Witwatersrand Supergroup consists of metamorphosed argillaceous and arenaceous lithological units deposited on the Kaapvaal Craton through successive depositional events over 3086 Ma ago [29]. The Witwatersrand Supergroup is divided into the shallower Central Rand Group and the deeper West Rand Group. The Johannesburg Dome and the Witwatersrand Supergroup are overlain by the Ventersdorp lavas and younger sedimentary units of the Palaeoproterozoic Transvaal and Phanerozoic Karoo Supergroups [30]. The presence of faults and shear zones indicates periods of uplift and fracturing that occurred after the dome's emplacement and the deposition of overlying sequences [29].

2.3. Climate and Hydrology

Johannesburg's temperate climate is characterized by warm, wet summers and cold, dry winters. Average daily maximum temperatures peak at 28 °C in January and drop to 17 °C in July. Rainfall is concentrated in the summer months, particularly from October to March, with thunderstorms being common. The mean annual rainfall ranges between 600 and 900 mm/year, with the months November to February generally receiving more than 100 mm each (see Figure 4).

Figure 2. Regional context of the study area within the Limpopo River catchment, on the border between the Highveld (grassland, >1500 m elevation) and Bushveld (savannah, <1500 m) of South Africa. The dashed rectangle shows the area of Figure 3.

The Little Jukskei is a perennial river and flows for approximately 29 km from 1670 to 1310 mamsl into the Jukskei River. Flow was less than 1 $m^3 \cdot s^{-1}$ daily average for most of 2021, especially during the dry season (May to September), with several highs in the rainy season over 2 $m^3 \cdot s^{-1}$ and a peak in January of more than 10 $m^3 \cdot s^{-1}$ daily average (see Figure 5).

2.4. Hydrogeology

There are no major, high-yielding aquifers underlying the study site, but significant groundwater resources do exist. There are four principal aquifer types in this region: fractured granite, fractured quartzite, weathered granite and surficial materials.

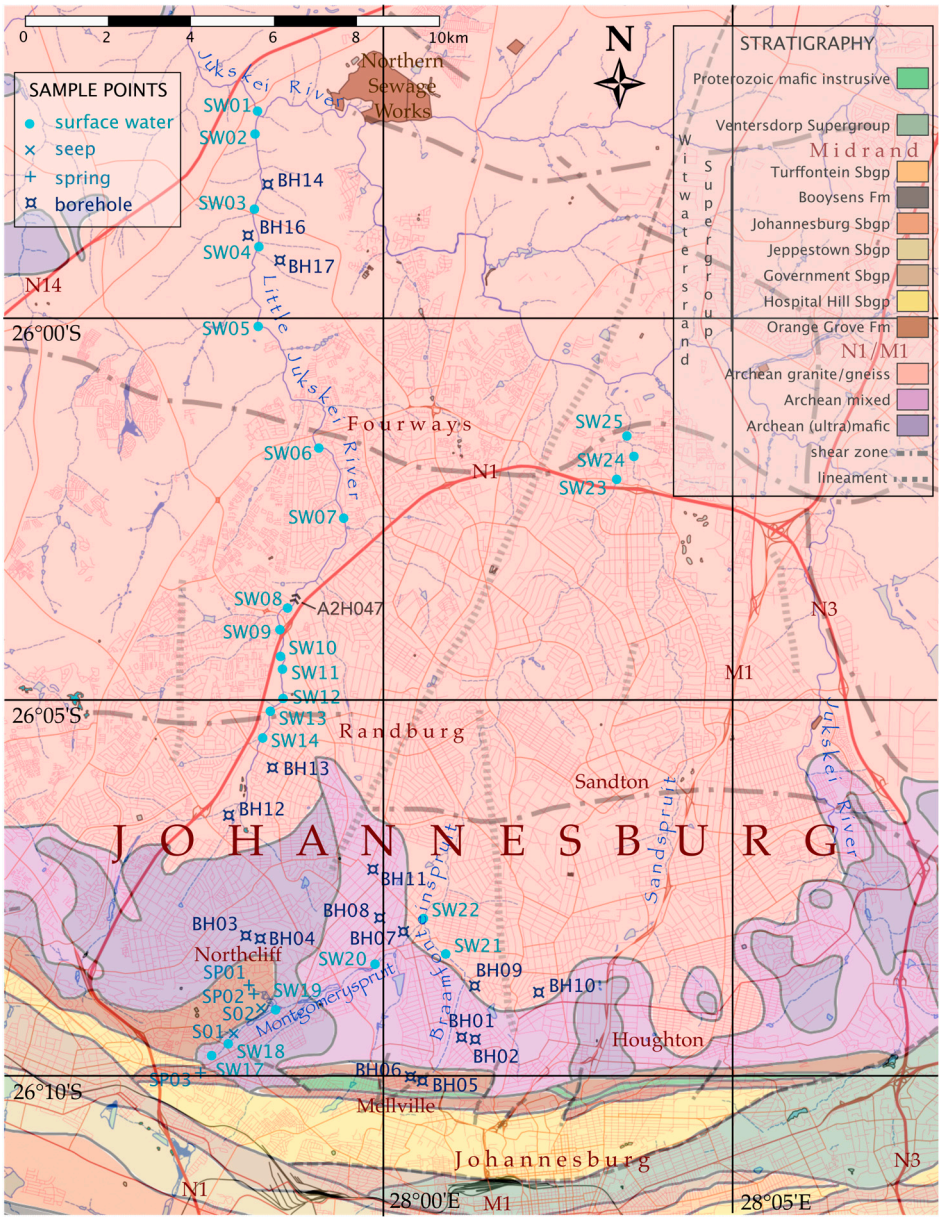

Figure 3. Map of the study area, including geology, rivers, roads and sample locations.

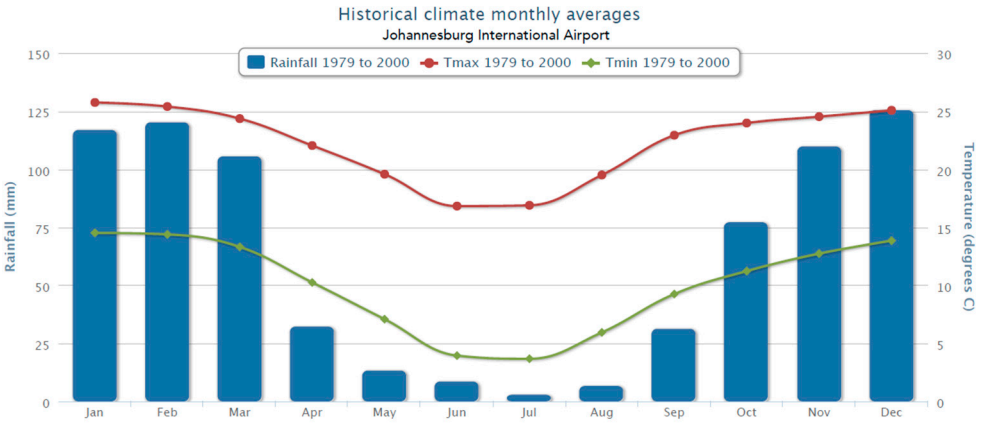

Figure 4. Climate of the study area. Johannesburg International Airport (now Oliver Tambo International Airport) is 20 km east of the study area and at a similar elevation (Source: CSAG 2024 [31]).

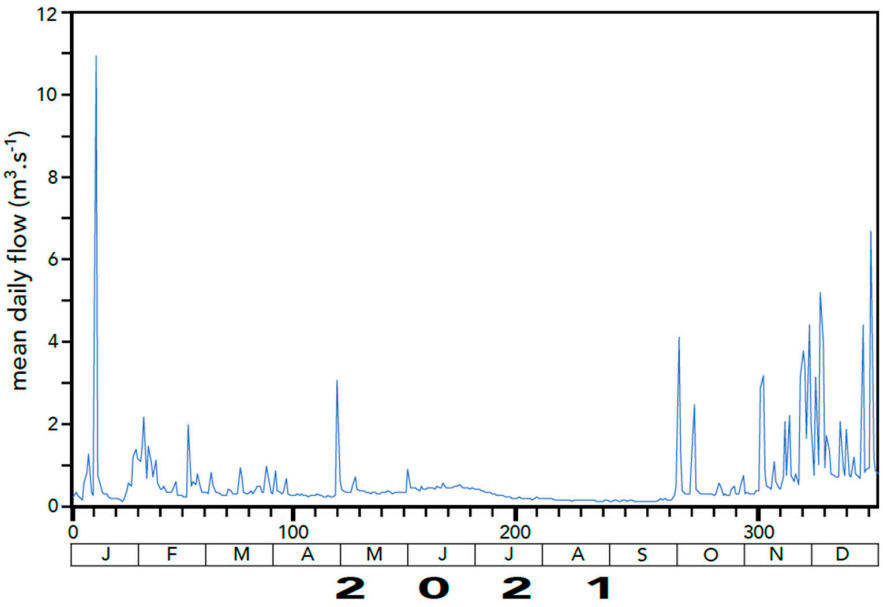

Figure 5. Mean daily flow in the Little Jukskei River in 2021 (Source: DWS, 2023 [32]), at flow gauge A2H047 (Figure 3).

Granitic fractured aquifers are formed with secondary structural features such as joints and faults, facilitating rapid recharge and offering moderate borehole yields ranging from 1 to 15 L/s. On the other hand, quartzite fractured aquifers extend to greater depths but provide limited yields, typically ranging from 0 to 1 L/s. The weathered zone aquifers originate from the weathering of crystalline rock and are typically unconfined to semi-confined, and connected to fractured aquifers [33]. High-yielding springs in the Witwatersrand Supergroup emerge at the interface between fractured quartzite and shale layers. The Albert's Farm Conservatory Spring exemplifies this phenomenon. Minor aquifers comprising unconsolidated sand and gravel, characterized by low yields, contribute to baseflow with a minimum recharge rate of 3% of mean annual precipitation. The diminished baseflow within the JRC is ascribed to the predominantly crystalline geology, the elevated position in the catchment, bordering a continental watershed, and the urbanized nature of the catchment [34].

3. Materials and Methods

3.1. Sampling

Groundwater, comprising privately owned boreholes, springs and seepages, and surface water were sampled along the Little Jukskei River, Montgomeryspruit, Braamfonteinspruit, Sandspruit and adjacent suburbs during 2020 and 2021 (see Figure 3). Sampling was conducted in the dry season in three campaigns. Finally, a high-resolution temporal campaign was conducted at the Albert's Farm Conservatory Spring, Montgomery Spring and Montgomeryspruit–stormwater runoff confluence at the start of the rainy season.

3.2. Measuring Radon and Field Parameters

Infield pH, EC (electrical conductivity) and temperature were measured using the EXTECH ExStik EC500 multimeter, calibrated and verified prior to use. Grab sampling was used for radon analysis, following the prescriptions of the RAD7 H_2O manual [35]; water samples were taken using 40 mL for boreholes and springs and 250 mL for surface water and seepage points. For boreholes, this entailed running the taps for several minutes, depending on the pumping frequency, as more recently pumped boreholes were presumed to require less purging. The glass vials were rinsed and filled by allowing overfill for twenty seconds before stoppering the vial as the tap ran. For surface water and springs, the glass vials were lowered at least 10 cm

below the surface before filling and stoppering the vial while submerged in water. Samples were stored in a cooler bag before analysis.

Radon analysis was done within 24 h of sampling using the RAD7 H_2O detector [35]. After starting, the machine was purged with atmosphere for 5 min to remove remnants of previous analyses, and then pumped in closed circulation through dessicant for 10–20 min to reduce the relative humidity to 6%. The sample vials were run for 5 min of aeration and counted for 30 min using the appropriate protocol setting for the respective volume. The minimum detection limit of 0.1 $Bq \cdot m^{-3}$ required purging for at least 20 min between each sample. The samples were analyzed in expected order of increasing radioactivity (surface water before groundwater) to reduce the potential for background contamination in subsequent samples.

3.3. Stable Isotopes

Samples of groundwater and surface water were also analysed for hydrogen and oxygen stable isotope compositions. The international standard Vienna Standard Mean Ocean Water (VSMOW) is used to report results against the SMOW scale. Because variations in the heavy-to-light isotope ratio are in the thousandths or hundredths, the sample is compared to a standard and reported as deviations in per mille (thousandths, ‰) from the standard, using the δ notation, as follows:

$$\delta^{18}O_{sample-}SMOW = [(^{18}O/^{16}O)_{sample}/(^{18}O/^{16}O)_{standard(SMOW)} - 1] \times 1000$$

and similarly for $^{2}H/^{1}H$.

Water sampling for stable isotope analysis entailed first rinsing 500 mL polypropylene bottles with the water of interest and then filling the bottles. The bottles were stored in a cooler box and transported to the iThemba laboratory at the University of the Witwatersrand, Johannesburg. Hydrogen and oxygen isotopes were analysed by mass spectrometry using the 2010 ThermoFisher Delta V Plus. Accuracy for $\delta^{2}H$ and $\delta^{18}O$ are ±1 and ±0.1 ‰, respectively.

3.4. FINIFLUX Model

The FINIFLUX model estimates groundwater flux by comparing radon concentrations between surface water and groundwater using the radon steady-state mass balance (Equation (1)). FINIFLUX solves the mass balance using an implicit finite solution [36]. Therefore, the solution is derived through a series of steps, with each step's solution being based on the solution obtained in the preceding step. The model is coupled with PEST, a parameter estimation software that estimates unknown parameters like groundwater influx and hyporheic exchange. The parameters are optimized by applying an algorithm that relies on the empirical measurements and numerical predictions to minimize the geometric shape function value [37].

FINIFLUX has been used to estimate groundwater input into a stream, similar to the application of the model in this study [10], as well as feeding into other models, for example for chemical interactions in the hyporheic zone [38,39]. As such, it is an accepted and widely used model and is appropriate for application in this study.

The Rn data was used for calculation of baseflow, whereas the $\delta^{2}H$ and $\delta^{18}O$ data was not. This is because these stable isotopes varied less than the Rn between groundwater and surface water, partly because the original values are less different, but mainly because Rn degasses from surface water and therefore groundwater inputs are more noticeable than for $\delta^{2}H$ or $\delta^{18}O$.

4. Results and Discussion

The results from this study are outlined in Tables 2 and 3 for groundwater and surface water, respectively.

Table 2. Water field parameters and isotope results of groundwater observation points in this study. Sample labels are prefaced as follows: BH for boreholes, S for seepages, SP for springs. EC = electrical conductivity, SD = standard deviation.

Sample	Latitude	Longitude	Depth Estimate	Date	δ^2H	$\delta^{18}O$	d-Excess	T	pH	EC	Rn Mean	Rn SD
	°S	°E	m bgl		‰	‰	‰	°C		$\mu S \cdot cm^{-1}$	$Bq \cdot m^{-3}$	$\pm Bq \cdot m^{-3}$
BH001	26.1629	28.0254	20	21 March	−15.9	−2.93	7.54	14.3	7.41	717	14,009	4160
BH002	26.1638	28.0247	20	21 March	−20.0	−3.75	10.0	14.4	7.26	889	6840	1470
BH003	26.1452	27.9757	30	21 March	−16.8	−3.04	7.52	14.7	7.40	154	2940	670
BH004	26.1442	27.9783	25	21 March	−18.4	−3.68	11.04	14.7	7.21	147	1330	439
BH005	26.1731	28.0082	10	21 March	−19.9	−4.04	12.42	17.4	7.33	321	18,006	3230
BH006	26.1734	28.0075	15	21 March	−7.4	−1.53	4.84	17.6	7.01	536	78,009	3350
BH007	26.1371	27.9981	10	21 March	−12.7	−3.21	12.98	16.1	7.36	154	58,007	4720
BH008	26.1362	27.9979		21 March	−13.4	−2.92	9.96	16.2	7.28	83	52,008	4140
BH009	26.1523	28.0241	20	21 March	−12.6	−2.74	9.32	15.3	7.12	221	26,006	3210
BH010	26.1539	28.0404	20	21 March	−18.5	−3.78	11.74	15.5	7.23	265	42,006	3430
BH011	26.1265	27.9968	120	21 March	−16.9	−3.57	11.66	16	7.55	527	196,000	9000
BH012	26.1127	27.9616	50	21 July	−14.5	−3.44	13.02	13.1	7.13	261	21,009	2320
BH013	26.1019	27.9678	40	21 July	−25.4	−4.78	12.84	19	7.41	145	174,000	10,000
BH014	25.9721	27.9666	20	21 July	−19.2	−3.71	10.48	14.1	7.43	761	2290	870
BH016	25.9834	27.9613	25	21 July	−22.8	−4.46	12.88	20.2	7.37	525	57,005	3330
BH017	25.9953	27.9769		21 July	−28.0	−5.27	14.16	21	7.56	154	70,000	1360
S01	26.16452	27.96506		21 August	−18.89	−3.77	11.27	16.6	-	370	910	377
S02	26.15933	27.97414		21 August	−15.72	−3.23	10.12	20.3	-	175	7322	1046
SP001	26.1552	27.9700		21 March	−13.8	−2.98	10.04	25.2	7.50	141	17,003	2130
				21 May	−16.8	−3.46	10.88	17.2	7.11	154	29,005	3620
				21 July	−17.3	−3.62	11.66	18	7.63	150	28,000	2170
				21 September	−14.6	−2.98	9.24	21.4	7.28	162	14,370	1060
SP002	26.1555	27.9702		21 March	–	–	-	19.8	6.62	158	30,007	5130
				21 May	–	–	-	25.6	7.47	144	38,004	4430
				21 July	–	–	-	17.2	7.61	130	41,003	3910
				21 September	–	–	-	18.3	7.30	131	33,000	4520
SP003	26.1697	27.96		21 March	−16.4	−4.32	18.16	22.3	7.41	103	3970	694
				21 July	−19.6	−3.81	10.88	26.1	7.40	121	2940	503
				21 September	−20.4	−3.86	10.48	17.4	7.57	144	4370	560
means					**−17.78**	**−3.61**	**11.01**	**18.22**	**7.37**	**274**	**36,875**	**2960**

Table 3. Water field parameters and isotope results of surface water observation points in this study.

Sample	Date	δ^2H	$\delta^{18}O$	d-Excess	EC	Rn Mean	Rn SD
		‰	‰	‰	$\mu S \cdot cm^{-1}$	$Bq \cdot m^{-3}$	$\pm Bq \cdot m^{-3}$
SW01	21 March	−16.6	−3.12	8.36	473	1678	179
	21 July	–	–	–	421	1567	208
	21 September	−15.8	−2.72	5.96	444	1080	117
SW02	21 March	−15.2	−2.71	6.48	468	1006	240
	21 July	–	–		422	1127	354
	21 September	−14.0	−2.16	3.28	451	988	321
SW03	21 March	−15.8	−3.02	8.36	460	414	198
	21 July	–	–		566	403	191
	21 September	−16.2	−3.39	10.92	421	376	84
SW04	21 March	−18.1	−3.06	6.38	506	512	265
	21 July	–	–	–	412	441	234
	21 September	−14.6	−2.48	5.24	447	562	129
SW05	21 September	−15.9	−2.66	5.38	422	403	111
SW06	21 September	−15.0	−2.38	4.04	472	1419	450
SW07	21 September	−14.4	−2.42	4.96	359	367	189
SW08	21 March	–	–	–	353	642	234
	21 July	−16.6	−2.93	6.84	362	705	198
	21 September	–	–		374	638	202
SW09	21 March	−14.8	−2.96	8.88	334	1870	750
	21 July	–	–	–	421	2001	767
SW10	21 March	−15.3	−2.98	8.54	373	2080	483
	21 July	–	–	–	365	2012	501
	21 September	−14.1	−2.89	9.02	291	2001	557
SW11	21 March	−15.1	−3.07	9.46	365	1040	417
	21 July	–	–		476	876	306
	21 September	−14.2	−2.91	9.08	321	921	261
SW12	21 March	−15.6	−2.95	8.0	363	1940	436
	21 July	–	–		374	1234	675
	21 September	−13.8	−3.03	10.44	403	1255	370
SW13	21 March	−15.5	−2.96	8.18	364	1250	481
	21 July	–	–	–	372	1116	527
SW14	21 March	−15.5	−2.97	8.26	366	830	279
	21 July	–	–	–	402	710	321
SW15	21 March	−15.8	−3.25	10.2	543	1250	970
SW16	21 March	−14.1	−3.0	9.9	385	1040	796
SW17	21 October	–	–	–	180	2530	830
SW18	21 July	−14.9	−3.15	10.3	394	796	224
SW19	21 March	−15.4	−2.97	8.36	491	877	142
SW20	20 August	−10.9	−2.28	7.31	480	1422	460
SW21	21 July	−14.1	−2.76	7.98	410	1240	425
SW22	21 July	−14.6	−2.77	7.56	437	1180	532
SW23	21 July	−15.5	−3.09	9.22	556	1660	679
SW24	21 March	–	–	–	409	416	208
SW25	21 March	−13.4	−2.49	6.52	392	479	115
means		−15.03	−2.85	7.78	411	1099	373

4.1. Charcterization of Groundwater and Surface Water

4.1.1. Groundwater

Groundwater and surface water in the study area displayed distinct characteristics reflective of the local geology and land use. Groundwater radon concentrations in the study area varied widely, ranging from 910 to 196,000 $Bq \cdot m^{-3}$, with an average of approximately

36,900 Bq·m^{-3}. This variability is attributed to heterogeneous distribution of uranium-bearing minerals and rock permeability variability.

The average radon concentration in groundwater in this study is higher than the 100–10,000 Bq·m^{-3} found in Cyprus [40] or the 8000–21000 Bq·m^{-3} in Japan [41] but less than the mean of 240,000 Bq·m^{-3} found in Poland [42]. The latter was, similarly to this study, an area underlain by gneiss and granite.

The highest radon concentration was recorded at BH013, located along a major structural lineament (see Figure 3), indicating enhanced radon migration through fractured zones. In contrast, boreholes such as BH014 showed low radon but high EC (see Figure 6), suggesting possible mixing with wastewater [43]. The radon concentrations of the seep (natural groundwater discharge points) samples are considerably lower than those of the borehole and spring samples, indicating a clear divide between the waters which have been significantly exposed to atmosphere and those which have not. Overall, elevated radon levels in groundwater are indicative of subsurface geological controls, particularly structural features that facilitate groundwater movement and radon transport.

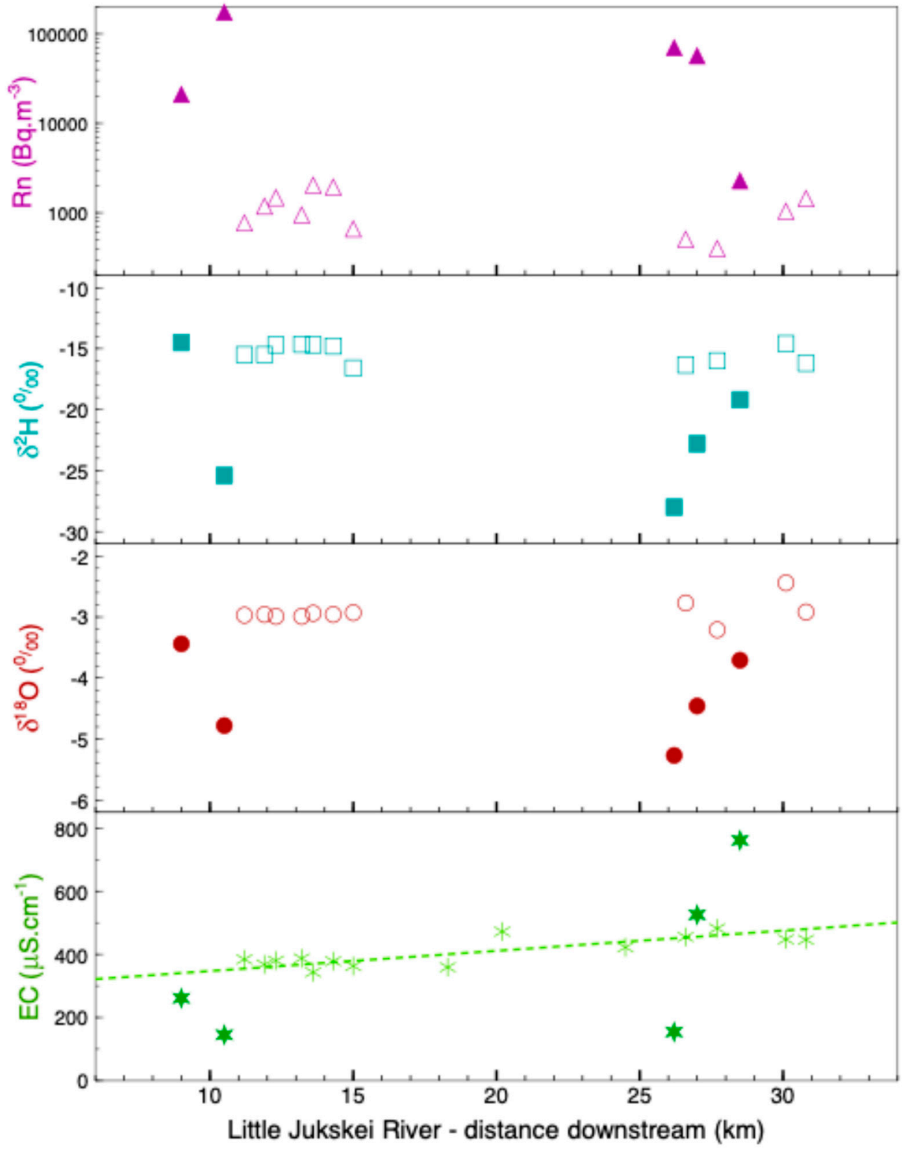

Figure 6. Radon concentration, δ^2H, δ^{18}O and electrical conductivity of water samples versus distance downstream in the Little Jukskei River. Locations with multiple samples taken over several months

have used the mean of those values. The radon data shows a clear difference between higher values for groundwater and lower ones for the river, enabling the use of radon to estimate baseflow. For δ^2H and $\delta^{18}O$, the differences are smaller, but suggest evaporative enrichment in the river. The trend line for EC vs. distance has the equation EC = 17 × km + 57, with Pearson's r of 0.53, indicating a mild positive correlation. Slight increases in both $\delta^{18}O$ and EC suggest evaporation with distance downstream. See main text for further discussion.

Stable isotope analysis revealed a wide spread of δ^2H and $\delta^{18}O$ values in groundwater. Outlier points, such as BH006, suggested localized influences from municipal water infrastructure [44]. The groundwater regression line in Figure 7 was calculated excluding this point. The slight shift of the groundwater points away from the Johannesburg Local Meteoric Water Line (JLMWL) suggests recharge occurs with minor evaporation during infiltration [39]. There is no correlation between Rn and δ^2H (Pearson's r = −0.16) or Rn and $\delta^{18}O$ (r = −0.17).

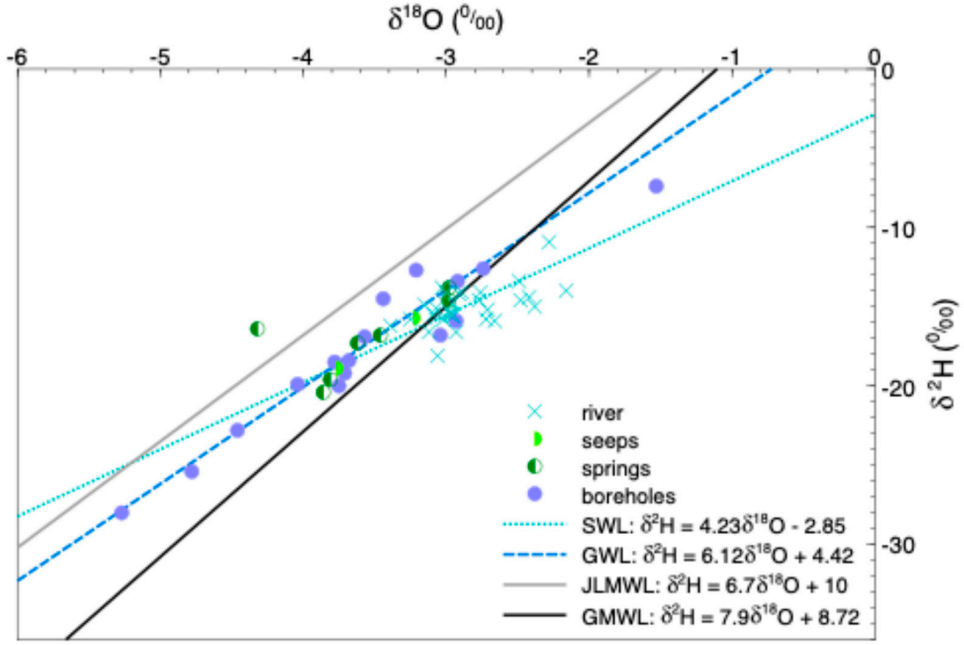

Figure 7. δ plot of all samples in this study, including groundwater (seeps, springs and boreholes) and surface water from the Little Jukskei River, Montgomeryspruit, Braamfonteinspruit and Sandspruit, as shown in Figure 3. Best fit lines for groundwater (GWL) and surface water (SWL), calculated with reduced major axis regression, have Pearson's r values of 0.91 and 0.57, respectively. The Johannesburg Local Meteoric Water Line is from Leketa et al. 2018 [45] and the Global Meteoric Water Line is from Terzer et al., 2013 [46].

Groundwater samples exhibited generally low EC values (mean ~274 $\mu S \cdot cm^{-1}$), consistent with the granitic geological setting, rapid recharge through fractures and minimal interaction with mineralized matrices [47–49]. Groundwater temperatures (13.1–12.1 °C, average 18.42 °C) were lower and more stable than surface water (14.6–28.7 °C, average 19.07 °C), suggesting that baseflow moderates stream temperatures, especially during dry periods. Post-rainfall decreases in groundwater pH, linked to acidic rainwater (pH 3.0–6.56) caused by natural CO_2 and anthropogenic pollutants (SOx, NOx, etc.), demonstrate recharge dynamics and hydrological connectivity.

4.1.2. Surfacewater

Surface water radon concentrations ranged from 367 to 2530 $Bq \cdot m^{-3}$, with an average of approximately 1100 $Bq \cdot m^{-3}$. These values were subject to high variability and marginal

errors, primarily due to natural radon degassing and sampling challenges. Elevated radon concentration levels are observed at specific points located downstream of groundwater discharge points. For example, there is an increase in radon concentration from SW19 (downstream S02) and similarly thereafter between SW20 and SW22 (4 km reach along Montgomery Spruit). The stream reach is only a few centimeters deep and thus prone to high degrees of degassing. Therefore, the relatively constant radon concentration indicates steady groundwater discharge along this reach or is representative of the background radon concentration.

Surface water isotopic signatures were more tightly clustered and aligned along a local evaporation line (LEL). The true LEL for a region will be plotted with points from water affected only by evaporation. In this case, the surface water line (SWL in graph) data is more clustered close to the local meteoric water line, reflecting some evaporation but also consistent groundwater contributions [24,25] (see Figure 7). The surface water regression line's moderate correlation (r = 0.57) and lack of a clear trend of isotopic enrichment downstream in the Little Jukskei River support the consistenst groundwater contribution and cumulative inputs of wastewater and stormwater. As for groundwater, there is no correlation in the surface water between Rn and δ^2H (Pearson's r = 0.15) or Rn and δ^{18}O (r = −0.09).

Surface water EC values were higher on average (~411 $\mu S \cdot cm^{-1}$), likely influenced by urban runoff and wastewater effluent [50]. A slight trend of increasing EC downstream is observed (see Figure 6), also likely due to evaporative concentration and wastewater and stormwater inputs. Surface water pH ranged from 7.12 to 7.91, indicating slightly basic conditions with relatively minor seasonal variation. This stability suggests a buffering effect from the various inputs.

4.2. Radon as a Tracer for Groundwater Input

Radon concentrations in groundwater varied widely (910 to 196,000 $Bq \cdot m^{-3}$), with elevated levels associated with structural lineaments and fractured zones. These zones represent preferential pathways for groundwater flow and radon transport. Groundwater discharge is localized along these zones and seepages.

Radon concentration along the Montgomeryspruit decreases in the first 700 m from its emergence at SP03, to SW18. While there is a considerable uncertainty overlap between the radon concentration at SW18 (796 ± 224 $Bq \cdot m^{-3}$) and the adjacent seepage S01 (910 ±377 $Bq \cdot m^{-3}$), S01 shows a higher mean concentration, which is to be expected for a soil or groundwater source, but the similarity to the surface water suggests that the S01 may have spent little time underground and could therefore be from a water pipe leak.

Seepage S02, located 1900 m further downstream of S01, shows a significantly higher radon concentration (7322 ± 1046 Bq/m^{-3}) relative to the stream, suggesting that it is fed by deeper groundwater. This high radon concentration and EC value, similar to SP01 (Alberts Farm Spring), suggest a connection between Alberts Farm Spring and the groundwater feeding S02. This is in line with the findings of [51], whose piezometric levels and stable isotope data indicated that interflow feeds Montgomeryspruit.

Spatial analysis indicated localized zones of enhanced baseflow along the Little Jukskei River, especially where structural features intersected the river, inferred from elevated radon concentrations in surface water (Section 4.3). Conversely, stretches with low radon concentrations suggest limited or no groundwater input, likely due to low hydraulic gradients and impermeable subsurface conditions.

4.3. Seasonal Trends and Baseflow Indicators

The FINIFLUX model shows decreasing groundwater inflow over time along the Little Jukskei River, from March to July to September 2021 (see Figure 8)—note the different *y*-axis scale for groundwater input. Groundwater inflow in the first 4180 m fluctuated

between 0.10×10^{-4} and 0.17×10^{-4} $m^3 \cdot m^{-1} \cdot s^{-1}$ between March and September 2021, with notable exceptions. These include a peak of 0.35×10^{-4} $m^3 \cdot m^{-1} \cdot s^{-1}$ in March between 3250 and 3660 m and no inflow between 3660 and 4180 m in September.

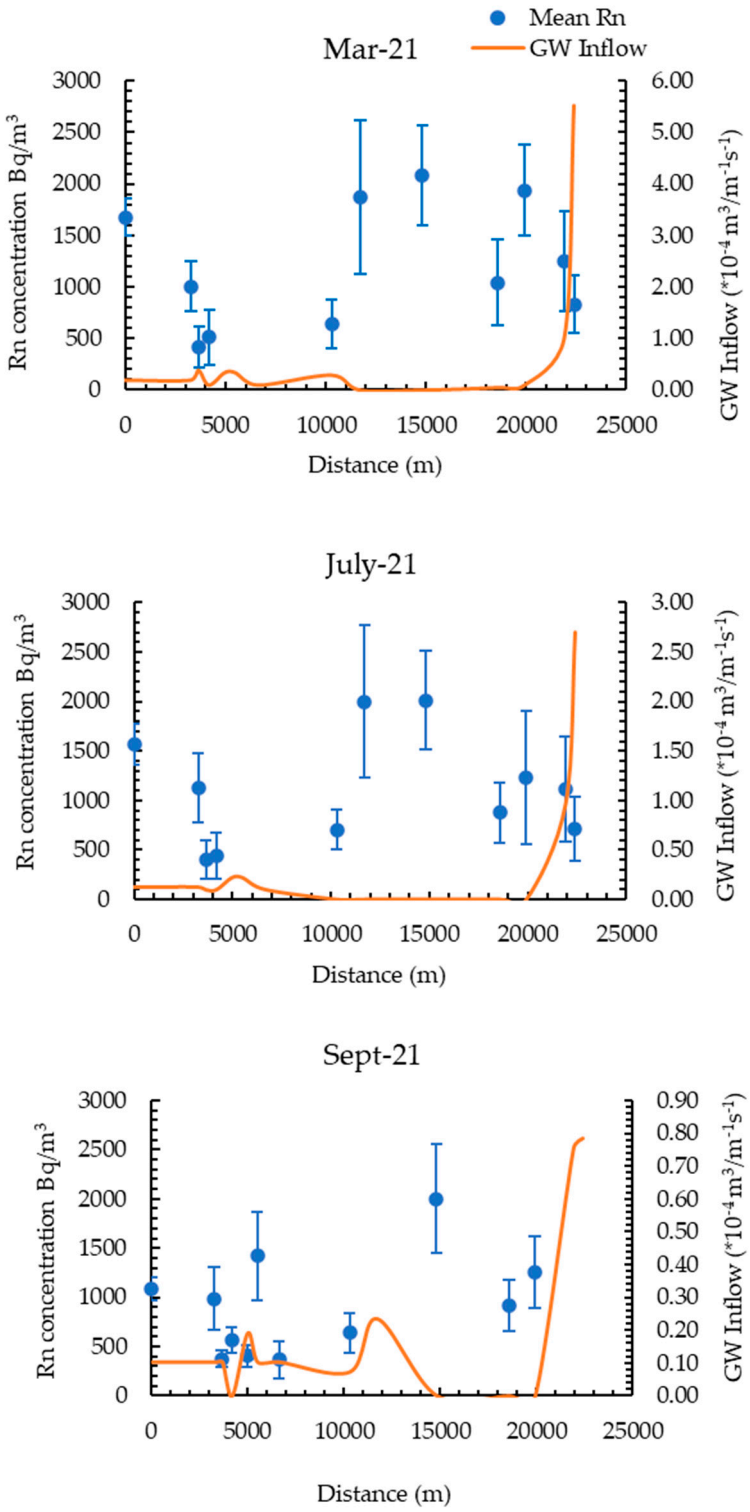

Figure 8. Measured radon concentration in surface water and predicted groundwater inflow from the FINIFLUX model, plotted against distance downstream in the Little Jukskei River. The same analyses and procedure have been conducted for three periods: March 2021 (**top**), July 2021 (**middle**) and September 2021 (**bottom**). Note the different *y*-axis scales for groundwater inflow, showing reducing levels of groundwater input from March to July to September. The spike in groundwater inflow at the downstream side is from a modelling artefact from being near the model boundary.

The FINIFLUX model was validated using measured radon concentrations from surface water and adjacent groundwater sources within the Little Jukskei River catchment. The model applied a least mean square error (LMSE) approach to minimize discrepancies between modelled and observed radon concentrations using a parameter estimation algorithm (PEST).

The correlation between modelled and measured radon concentrations in March and July showed high correlation (r = 0.95–0.995), indicating strong agreement between modelled and measured radon activities. The results for the September campaign showed the lowest r values (<0.95), attributed to the lower overall radon concentrations observed during that period. This weakened model optimization likely resulted in the underestimation of groundwater inflow. Urban stormwater runoff, especially during the onset of the rainy season, may have diluted radon levels or caused short-term spikes, complicating the interpretation of the data. Additionally, wastewater effluent and infrastructure such as sewers and impervious surfaces can mask or alter natural groundwater signals, as seen when stable isotopes indicated limited groundwater–surface water interaction that may have been obscured by urban wastewater inputs. Furthermore, access and morphological constraints in urban river sections required extrapolation of parameters like flow rate, introducing further uncertainty into the model.

The study reveals a trend in groundwater inflow along the Little Jukskei River based on surface water radon concentration patterns across three campaigns. The March campaign indicates the highest groundwater inflow, attributed to increased baseflow following the rainy season, whereas the September campaign, at the end of the dry season, indicates the lowest groundwater input. This suggests a seasonal fluctuation in groundwater levels, receding in the dry season and rising during the rainy season, consistent with findings in similar geological settings elsewhere, such as southwestern Nigeria [52].

This seasonal pattern is consistent with a fluctuating water table and limited aquifer storage capacity in the fractured granitic geology of the area. Overall, baseflow was found to be temporally variable, also controlled by the structural geology.

4.4. Isotope Patterns and Recharge Dynamics

Groundwater isotope values clustered below the Johannesburg Local Meteoric Water Line (JLMWL), indicating recharge with minor evaporation during infiltration. Groundwater exhibits a wide range of isotopic compositions, indicating that recharge takes place during both typical and atypical rainfall conditions—the latter involving extreme events that may result in more negative delta values [53–55]. d-excess values further corroborated these findings, distinguishing between evaporated surface waters and spring-fed contributions.

Anomalous d-excess values in the Montgomery Spring during March indicated mixing with urban runoff, while consistent d-excess at the Albert's Farm Spring confirmed a groundwater origin. These patterns underscore the value of combined isotope and field parameter analysis in tracing water sources.

Springs such as Albert's Farm (SP001) showed higher radon and EC values in the dry season, attributed to longer residence times and increased mineralisation. In contrast, reduced EC in the rainy season reflected dilution from recharge. This dynamic was mirrored in surface water, though signals were often masked by urban wastewater inputs.

4.5. Structural and Geologic Controls

The fractured crystalline aquifers of the Johannesburg Dome provide limited storage and transmissivity, yet structural lineaments serve as high-permeability zones enabling focused discharge. Boreholes located along these features exhibited higher radon levels,

suggesting enhanced connectivity to deeper groundwater. These structurally controlled zones also influence pathological risk in borehole water due to elevated radon levels.

The flat topography of the sub-catchment further limits hydraulic gradients [56], reducing overall groundwater discharge potential except where aided by structural conduits. Fractures and faults act as primary pathways for groundwater flow and enable rapid recharge.

4.6. Implications for Urban Hydrology and Water Management

In regions with highly permeable geology, groundwater domination in streamflow during dry seasons is common. However, the impermeable underlying geology of Johannesburg suggests surface water-dominated streamflow along the Little Jukskei River, supported by tributaries. Similar detachment of surface water from groundwater is observed in environments like western Niger, where runoff rates are high due to thin soil profiles overlying granitic areas [56]. Exposure of rock outcrops along the Little Jukskei River indicates thin soil profiles and streambed sands, contributing to increased runoff rates and surface water dominance. These findings underscore the complex interplay between groundwater and surface water dynamics in the studied area.

The study demonstrates that urban baseflow is spatially and temporally variable, influenced by seasonal recharge, structural controls and urban infrastructure. The low baseflow index (~20.8%) for the Little Jukskei River, compared to the national average (~31%), confirms a weak groundwater contribution overall, yet with localized zones of significance [57,58].

Maintaining baseflow is critical for ecological health and water quality in urban streams, especially during dry seasons. The findings suggest that preserving recharge zones and mitigating infrastructure leaks and runoff pollution should be priorities for urban water governance. Further, rapid assessment tools like radon and EC, complemented by stable isotopes, provide robust and practical methods for urban hydrogeological investigations.

5. Conclusions

Electrical conductivity (EC) revealed a seasonal pattern of higher EC during the dry season and lower in the rainy season, a slight downstream increase in EC, possibly due to evaporation, and a generally low EC in groundwater, suggesting fast groundwater flow through fractures, limiting rock dissolution.

Hydrogen and oxygen stable isotopes identified a leaking water pipe that feeds BH006, due to the outlying nature of this point and its close match to municipal water. Springs, seeps and boreholes all have a wide and overlapping range of δ values, suggesting varied recharge, such as seasonal in wet years and event-based after large storms. Surface water δ values to lie on an evaporation line, but close to groundwater and the LMWL, indicating only slight evaporation, reinforcing the conclusion from EC. The clustering of the stable isotope data and lack of a clear downstream-evaporation trend suggest regular groundwater input into the stream.

Radon measurements in groundwater varied, suggesting different groundwater types, most likely caused by the presence of fractures with preferential flow and radon migration along those fractures. The highest value, 196,000 $Bq \cdot m^{-3}$, from BH013 is along the extension of a mapped lineament, and is a slight cause for concern if used indoors. The FINIFLUX model shows decreasing baseflow into the Little Jukskei River as the dry season proceeds, from March to July to September 2021. This proves that the water table fluctuates seasonally. The generally low baseflow quantities are partially due to the low hydraulic gradients in the landscape and the poor basement aquifers, but are moderated by the presence of

fractures, allowing more substantial volumes of groundwater to flow into the river where these structural features intersect the streamline.

Urban environments are challenging due to access to private or public land and security issues with leaving any monitoring equipment in place. Radon and EC analyses, both with quick results, are useful and can be performed in response to weather events. Stable isotopes, although taking longer to obtain results, add substantial value. Tritium and more novel tracers, such as noble gases or CFCs, may provide even further enlightenment, as would longer-term measurements of the same analytes used in this study, to capture different years with different weather conditions and develop a longer time series. Precipitation monitoring for stable isotopes would also be valuable.

The reliance of the Jukskei River on baseflow, especially to sustain the river during the dry season, demands that groundwater be understood better to ensure the resource is not depleted, resulting in drying of the river, affecting downstream users, including the environment. Additionally, the water quality of groundwater may be better than urban runoff, and so help maintain reasonable water quality in the river. There is much potential for further study of the urban water cycle in Johannesburg, to ensure sustainability of the groundwater resource and protection of the surface water ecosystem.

More generally, this study proves that quick, readily available and fairly cheap methods are useful for studying surface water and groundwater in urban areas. This is a vital necessity as cities increase in size and their impacts on water resources, the environment and humans become greater. Future work should include longer-term monitoring, incorporation of additional tracers (e.g., tritium, noble gases), and dedicated precipitation sampling to refine understanding of recharge sources and improve predictive modelling under different climate and land-use scenarios.

Author Contributions: K.D.: fieldwork, analysis, interpretation and writing. R.D.: conceptualisation, fieldwork, analysis, interpretation, writing and funding. F.K.: fieldwork and analysis. All authors have read and agreed to the published version of the manuscript.

Funding: The South African National Nuclear Regulator provided funds for this work—project number CNSS0117-A5-UP.

Data Availability Statement: The data for this study is given in tables within the article.

Conflicts of Interest: The authors declare no conflicts of interest.

Abbreviations

The following abbreviations are used in this manuscript.

BFI	baseflow index
CFCs	chlorofluorocarbons
EC	electrical conductivity
GWL	groundwater line
JRC	Jukskei River Catchment
LEL	local evaporation line
SMOW	Standard Mean Ocean Water
SWL	surface water line

References

1. Charters, F.J.; Cochrane, T.A.; O'Sullivan, A.D. The influence of urban surface type and characteristics on runoff water quality. *Sci. Total Environ.* **2021**, *755*, 142470. [CrossRef] [PubMed]
2. Barnes, M.L.; Welty, C.; Miller, A.J. Impacts of development pattern on urban groundwater flow regime. *Water Resour. Res.* **2018**, *54*, 5198–5212. [CrossRef]

3. O'Driscoll, M.; Clinton, S.; Jefferson, A.; Manda, A.; McMillan, S. Urbanization effects on watershed hydrology and in-stream processes in the southern United States. *Water* **2010**, *2*, 605–648. [CrossRef]
4. Kuhlemann, L.M.; Tetzlaff, D.; Soulsby, C. Urban water systems under climate stress: An isotopic perspective from Berlin, Germany. *Hydrol. Process.* **2020**, *34*, 3758–3776. [CrossRef]
5. Fleckenstein, J.H.; Krause, S.; Hannah, D.M.; Boano, F. Groundwater-surface water interactions: New methods and models to improve understanding of processes and dynamics. *Adv. Water Resour.* **2010**, *33*, 1291–1295. [CrossRef]
6. Boulton, A.J.; Datry, T.; Kasahara, T.; Mutz, M.; Stanford, J. Ecology and management of the hyporheic zone: Stream-groundwater interactions of running waters and their floodplains. *J. N. Am. Benthol. Soc.* **2010**, *29*, 26–40. [CrossRef]
7. Leibowitz, S.; Comeleo, R.; Wigington, P., Jr.; Weaver, C.; Morefield, P.; Sproles, E.; Ebersole, J. Hydrologic landscape classification evaluates streamflow vulnerability to climate change in Oregon, USA. *Hydrol. Earth Syst. Sci.* **2014**, *18*, 3367–3392. [CrossRef]
8. Kuhlemann, L.M.; Tetzlaff, D.; Soulsby, C. Spatio-temporal variations in stable isotopes in per-urban catchments: A preliminary assessment of potential and challenges in assessing streamflow sources. *J. Hydrol.* **2021**, *600*, 126685. [CrossRef]
9. Marx, C.; Tetzlaff, D.; Hinkelmann, R.; Soulsby, C. Isotope hydrology and water sources in a heavily urbanized stream. *Hydrol. Process.* **2021**, *35*, e14377. [CrossRef]
10. Schubert, M.; Siebert, C.; Knoeller, K.; Roediger, R.; Schmidt, A.; Gilfedder, B. Investigating groundwater discharge into a major river under low flow conditions based on a radon mass balance supported by tritium data. *Water* **2020**, *12*, 2838. [CrossRef]
11. Gilfedder, B.S.; Frei, S.; Hoffman, H.; Cartwright, I. Groundwater discharge to wetlands driven by storm and flood events: Quantification using continuous radon-222 and electrical conductivity measurements and dynamic mass-balance modelling. *Geochim. Cosmochim. Acta* **2015**, *165*, 161–177. [CrossRef]
12. Cook, P.G.; Wood, C.; White, T.; Simmons, C.T.; Fass, T.; Brunner, P. Groundwater inflow to a shallow, poorly-mixed wetland estimated from a mass balance of radon. *J. Hydrol.* **2008**, *354*, 213–226. [CrossRef]
13. Burnett, W.C.; Dulaiova, H. Estimating the dynamics of groundwater input into the coastal zone via continuous radon-222 measurements. *J. Environ. Radioact.* **2003**, *69*, 21–35. [CrossRef]
14. Strydom, T.; Nel, J.M.; Nel, M.; Petersen, R.M.; Ramjukadh, C.L. The use of Radon (Rn222) isotopes to detect groundwater discharge in streams draining Table Mountain Group (TMG) aquifers. *Water SA* **2021**, *47*, 194–199. [CrossRef]
15. Jasechko, S. Global Isotope Hydrogeology-Review. *Rev. Geophys.* **2019**, *57*, 835–965. [CrossRef]
16. Soulsby, C.; Birkel, C.; Geris, J.; Tetzlaff, D. Spatial aggregation of time-variant stream water ages in urbanizing catchments. *Hydrol. Process.* **2015**, *29*, 3038–3050. [CrossRef]
17. Rodriguez, F.; Delliou, A.L.L.; Andrieu, H.; Gironas, J. Groundwater contribution to sewer network baseflow in an urban catchment-case study of Pin Sec catchment, Nantes, France. *Water* **2020**, *12*, 689. [CrossRef]
18. Le Maitre, D.C.; Colvin, C. Assessment of the contribution of groundwater discharges to rivers using monthly flow statistics and flow seasonality. *Water SA* **2008**, *34*, 549–564. [CrossRef]
19. Yi, P.; Luo, H.; Chen, L.; Yu, Z.; Jin, H.; Chen, X.; Wan, C.; Aldahan, A.; Zheng, M.; Hu, Q. Evaluation of groundwater discharge into surface water by using radon-222 and the source area of the Yellow River, Qinghai, Tibet Plateau. *J. Environ. Radioact.* **2018**, *192*, 257–266. [CrossRef] [PubMed]
20. Bezuidenhout, J. Estimating indoor radon concentrations based on the uranium content of geological units in South Africa. *J. Environ. Radioact.* **2021**, *234*, 106647. [CrossRef]
21. Yang, J.; Yu, Z.; Yi, P.; Frape, S.K.; Gong, M.; Zhang, Y. Evaluation of surface water and groundwater interactions in the upstream Kui River and Yunlong Lake, Xuzhou, China. *J. Hydrol.* **2020**, *583*, 124549. [CrossRef]
22. Lamontagne, S.; Kirby, J.; Johnston, C. Groundwater-surface water connectivity in a chain of ponds semiarid river. *Hydrol. Process.* **2021**, *35*, e14129. [CrossRef]
23. Cartwright, I.; Gilfedder, B. Mapping and quantifying groundwater inflows to Deep Creek (Marybyrnong catchment, SE Australia) using ^{222}Rn: Implications for protecting groundwater dependant ecosystems. *Appl. Geochem.* **2015**, *52*, 118–129. [CrossRef]
24. Diamond, R.E. *Stable Isotope Hydrology*; The Groundwater Project: Guelph, ON, Canada, 2022.
25. Clark, I.D.; Fritz, P. *Environmental Isotopes in Hydrogeology*; CRC Press: Boca Raton, FL, USA, 2013.
26. Poujol, M.; Anhaeusser, C. The Johanneburg Dome, South Africa: New single zircon U-Pb isotopic evidence for early Archaean granite-greenstone development within the central Kaapvaal Craton. *Precambrian Res.* **2001**, *108*, 139–157. [CrossRef]
27. Anhaeusser, C. Palaeo- Meso- and Neoarchaean granite-greenstone basement geology and related rocks of the central and western Kaapvaal Craton, South Africa. In *The Archaean Geology of the Kaapvaal Craton, Southern Africa, Regional Geology Reviews*; Springer: Berlin/Heidelberg, Germany, 2019; Volume 1, pp. 55–81.
28. Prevec, S.A.; Anhaeusser, C.R.; Poujol, M. Evidence for Archaean lamprophyre from the Kaapvaal Craton, South Africa. *S. Afr. J. Sci.* **2004**, *100*, 549–555.
29. McCarthy, T. *The Story of Earth and Life: A Southern African Perspective on a 4.6 Billion Year Journey*; Penguin Random House: Midrand, South Africa, 2013.

30. Eriksson, P.G.; Altermann, W.; Hartzer, F.J. *The Geology of South Africa*; Number 10; Geological Society of South Africa and Council for Geoscience: Pretoria, South Africa, 2006; Chapter: The Transvaal Supergroup and its precursors; pp. 237–260.
31. CSAG Climate Systems Analysis Group. 2024. Available online: https://cip.csag.uct.ac.za/ (accessed on 4 February 2024).
32. DWS Department of Water and Sanitation. 2023. Available online: https://www.dws.gov.za/hydrology/Verified/HyDataSets.aspx?Station=A2H047 (accessed on 12 August 2023).
33. Barnard, H. *An Explanation of the 1:500,000 General Hydrogeological Map: Johannesburg 2526*; Department of Water Affairs & Forestry: Pretoria, South Africa, 2000.
34. Leketa, K.; Abiye, T.; Zondi, S.; Butler, M. Assessing groundwater recharge in crystalline and karstic aquifers of the Upper Crocodile River basin, Johannesburg, South Africa. *Groundw. Sustain. Dev.* **2019**, *8*, 31–40. [CrossRef]
35. Durridge. *RAD7 H_2O Radon in Water Accessory*; Owner's manual; Durridge Inc.: Billerica, MA, USA, 2018.
36. Frei, S.; Gilfedder, B.S. FINIFLUX: An implicit finite element model for quantification of groundwater fluxes and hyporheic exchange in streams and rivers using radon. *Water Resour. Res.* **2015**, *51*, 6776–6786. [CrossRef]
37. Doherty, J.; Hunt, R.J.; Tonkin, M.J. *Approached to Highly Parameterized Inversion: A Guide to Using PEST for Model Parameter and Predictive Uncertainty Analysis*; Scientific Investigations Report 5211; USGS: Reston, VA, USA, 2010.
38. Pittroff, M.; Frei, S.; Gilfedder, B. Quantifying nitrate and oxygen reduction rates in the hyporheic zone using ^{222}Rn to upscale biogeochemical turnover in rivers. *Water Resour. Res.* **2017**, *53*, 563–579. [CrossRef]
39. Cook, P.G.; Herczeg, A.L. (Eds.) *Environmental Tracers in Subsurface Flow*; Springer Science and Business Media: New York, NY, USA, 2012.
40. Kiliari, T.; Tsiaili, A.; Pashalidis, I. Lithological and seasonal variations in radon concentrations 534in Cypriot groundwaters. *J. Radioanal. Nucl. Chem.* **2010**, *284*, 553–556. [CrossRef]
41. Tsunomori, R.; Shimodate, T.; Ide, T.; Tanaka, H. Radon concentration distributions in shallow and deep groundwater around the Tachikawa fault zone. *J. Environ. Radioact.* **2017**, *172*, 106–112. [CrossRef]
42. Przylibski, T.A.; Mamont-Ciesla, K.; Kusyk, M.; Dorda, J.; Kozlowska, B. Radon concentrations in groundwaters of the Polish part of the Sudety Mountains (SW Poland). *J. Environ. Radioact.* **2004**, *75*, 193–209. [CrossRef]
43. Hoorzook, K.B.; Pieterse, A.; Heine, L.; Barnard, T.G.; van Rensberg, N.J. Soul of the Jukskei River: The extent of bacterial contamination in the Jukskei River in Gauteng Province, South Africa. *Int. J. Environ. Res. Public Health* **2021**, *18*, 8537. [CrossRef]
44. West, A.G.; February, E.C.; Bowen, G.J. Spatial analysis of hydrogen and oxygen stable isotopes ("isoscapes") in groundwater and tap water across South Africa. *J. Geochem. Explor.* **2014**, *145*, 213–222. [CrossRef]
45. Leketa, K.; Abiye, T.; Butler, M. Characterisation of groundwater recharge conditions and flow mechanisms in bedrock aquifers of the Johannesburg area, South Africa. *Environ. Earth Sci.* **2018**, *77*, 727. [CrossRef]
46. Terzer, S.; Wassenaar, L.I.; Araguas-Araguas, L.J.; Aggarwal, P.K. Global isoscapes for δ^{18}O and δ^{2}H in precipitation: Improved prediction using regionalized climatic regression models. *Hydrol. Earth Syst. Sci.* **2013**, *17*, 4713–4728. [CrossRef]
47. Jaunat, J.; Huneau, F.; Dupuy, A.; Celle-Jeanton, H.; Vergnaud-Ayraud, V.; Aquilina, L.; Labasque, R.; Coustumer, P.L. Hydrochemical data and groundwater dating to infer differential flowpaths through weathered profiles of a fractured aquifer. *Appl. Geochem.* **2012**, *27*, 2053–2067. [CrossRef]
48. Dhakate, R.; Singh, V. Identification of water-bearing fractured zones using electrical conductivity logging in granitic terrain, Andhra Pradesh, India. *Curr. Sci.* **2008**, *95*, 1060–1066.
49. Cook, P.G. *A Guide to Regional Groundwater Flow in Fractured Rock Aquifers*; CSIRO Land and Water: Glen Osmond, South Australia, 2003.
50. McCallum, J.L.; Cook, P.G.; Berhane, D.; Rumpf, C.; McMahon, G.A. Quantifying groundwater flows to streams using differential flow gaugings and water chemistry. *J. Hydrol.* **2012**, *416*, 118–132. [CrossRef]
51. Leketa, K.; Abiye, T. Using environmental tracers to characterize groundwater flow mechanisms in the fractured crystalline and karst aquifers in Upper Crocodile River basin, Johannesburg, South Africa. *Hydrology* **2021**, *8*, 50. [CrossRef]
52. Ogunkoya, O.; Adejuwon, J.; Jeje, L. Runoff response to basin parameters in southwestern Nigeria. *J. Hydrol.* **1984**, *72*, 67–84. [CrossRef]
53. Vogel, J.; van Urk, H. Isotopic composition of groundwater in semi-arid regions of southern Africa. *J. Hydrol.* **1975**, *25*, 23–36. [CrossRef]
54. Diamond, R.E.; Harris, C. Stable isotope constraints on hydrostratigraphy and aquifer connectivity in the Table Mountain Group. *S. Afr. J. Geol.* **2019**, *122*, 317–330. [CrossRef]
55. Carlier, C.; Wirth, S.B.; Cochand, F.; Hunkeler, D.; Brunner, P. Geology controls streamflow dynamics. *J. Hydrol.* **2018**, *566*, 756–769. [CrossRef]
56. Abdou, M.M.; Vandervaere, J.P.; Descroix, L.; Moussa, I.B. Comparative hydrodynamic study of granitic and sedimentary catchments in Western Niger. *Hydrol. Sci. J.* **2021**, *66*, 1541–1551. [CrossRef]

57. Smakhtin, V.U. Low flow hydrology: A review. *J. Hydrol.* **2001**, *240*, 147–186. [CrossRef]
58. Mayer, T.D.; Naman, S.W. Streamflow response to climate as influenced by geology and elevation. *J. Am. Water Resour. Assoc.* **2011**, *47*, 724–738. [CrossRef]